Dynamical stability of an ion in a linear trap as a solid-state problem of electron localization

G. P. Berman,[1] A. R. Bishop,[1] D. F. V. James,[1] R. J. Hughes,[2] and D. I. Kamenev[1,3]
[1]*Theoretical Division, Los Alamos National Laboratory, Los Alamos, New Mexico 87545*
[2]*Physics Division P-23, MS H-803, Los Alamos National Laboratory, Los Alamos, New Mexico 87545*
[3]*Center for Nonlinear Studies, MS B-258, Los Alamos National Laboratory, Los Alamos, New Mexico 87545*
(Received 28 November 2000; published 5 October 2001)

When an ion confined in a linear ion trap interacts with a coherent laser field, the internal degrees of freedom, related to the electron transitions, couple to the vibrational degree of freedom of the ion. As a result of this interaction, the quantum dynamics of the vibrational degree of freedom becomes complicated, and in some ranges of parameters even chaotic. We analyze the vibrational ion dynamics using a formal analogy with the solid-state problem of electron localization. In particular, we show how the resonant approximation used in analysis of the ion dynamics, leads to a transition from a two-dimensional (2D) to a one-dimensional problem (1D) of electron localization. The localization length in the solid-state problem is estimated in cases of weak and strong interaction between the sites of the 2D cell by using the methods of resonance perturbation theory, common in analysis of 1D time-dependent dynamical systems. We show that the localization length can be used as an indicator of the effective temperature of the trapped ion, which can be experimentally measured.

DOI: 10.1103/PhysRevA.64.053406 PACS number(s): 32.80.Pj, 05.45.Mt, 42.50.Vk

I. INTRODUCTION

The problem of quantum dynamics for Hamiltonian systems with time-periodic perturbation can be formulated in terms of an equivalent solid-state problem of electron localization on a lattice. Such kinds of connections were discussed for different models in [1,2] (see also references therein). However, most results are obtained for quantum kicked systems, such as a quantum kicked rotor or a quantum kicked oscillator. These systems are convenient for both analytical and numerical analysis because instead of differential equations one can use discrete quantum maps. At the same time, the existence of periodic kicks suggests that the external field involves an infinite number of harmonics with equal amplitudes. In more common physical situations, there are only a few harmonics in the perturbation. In particular, such a situation occurs when an ion trapped in a linear ion trap interacts with two laser fields with close frequencies [3]. In this case, the internal degree of freedom of the ion (related to the electron dynamics) interacts with the vibrational degree of freedom. This interaction can result in complicated and even chaotic dynamics of the vibrational degree of freedom of the ion. The analysis of the stability of the ion in this system can be performed using a model of a quantum harmonic oscillator perturbed by a monochromatic wave [3].

In this paper we show that the problem of stability of the monochromatically perturbed oscillator can be formulated in terms of localization of an electron in a two-dimensional (2D) solid state system. The resonance approximation, common in treatment of time-periodic systems, is used to reduce the effective dimensionality of the solid-state model in the case of relatively small interaction of the ion with the laser field. In order to compare two completely different systems, a similarity in the formal description of the time-periodic system and a space-periodic solid state is exploited; namely, in the time-dependent system we use the time-periodicity of the perturbation and employ a Floquet formalism, while in the solid-state system we exploit the space periodicity and use the Bloch theorem.

The paper is organized as follows. In Sec. II we describe the model used for description of an ion trapped in a linear ion trap and interacting with two laser fields with close frequencies. In Sec. III, we discuss the general procedure that allows us to treat a 1D time-periodic system on the same basis as a 2D solid-state model. In the case of a small perturbation, the resonance approximation is used in Sec. IV to decrease the effective dimensionality of the solid-state system from two to one. The localization length in the solid-state model is estimated in Sec. V by calculating the size of the chaotic region in the corresponding time-periodic system, in the situation when the interaction between the sites of the solid state is strong. In Sec. VI we discuss a connection of the localization properties of our system with the effective temperature of an ion which can be measured experimentally. Concluding remarks are given in Sec. VIII.

II. THE VIBRATIONAL HAMILTONIAN

In the following [3], we assume that two laser beams, designated the pump (p) and the Stokes (s), with slightly different frequencies ω_p and ω_s, respectively, interact with an ion trapped in a linear ion trap. Both beams are assumed to be plane polarized in the z direction with the amplitudes of the electric field $\mathcal{E}_z^{(p)}$ and $\mathcal{E}_z^{(s)}$, and the wave vectors $\mathbf{k}_p$ and $\mathbf{k}_s$. The Hamiltonian, including the effect of the harmonic evolution of the ion along the weak axis of the trap (but excluding the internal free evolution), is

$$\hat{\mathcal{H}}=\frac{\hat{p}^2}{2M}+\frac{M\omega^2\hat{x}^2}{2}+\frac{\varepsilon}{k}\cos(k\hat{x}-\Omega t), \tag{1}$$

where $\hat{p}$ and $\hat{x}$ are the x-components of the momentum and the coordinate of the ion, t is the time, M is the mass of the ion, ω is the frequency of the ion vibrations in the linear trap, $\varepsilon=2\chi k|\mathcal{E}_z^{(p)}\mathcal{E}_z^{(s)*}|$, $\Omega=\omega_p-\omega_s$, $k=(\mathbf{k}_p-\mathbf{k}_s)\cdot\mathbf{e}_x$, $\mathbf{e}_x$ is a

unit vector in the x direction, and $\chi = A\pi\epsilon_0/4\nu^3\Delta$ (ν and A being, respectively, the wavenumber and the Einstein A coefficient for the transition between the upper and lower manifolds, Δ the laser detuning, and ϵ_0 the permitivity of free space).

In the dimensionless form the Hamiltonian (1) reads

$$\hat{H} = \frac{\hat{\mathcal{H}}}{(M\omega^2/k^2)} = -\frac{h^2}{2}\frac{\partial^2}{\partial X^2} + \frac{X^2}{2} + \epsilon\cos(X-\mu\tau)$$
$$= \hat{H}_0 + V(X,\tau), \tag{2}$$

where $\hat{H}_0$ is the Hamiltonian of a linear oscillator,

$$X = kx, \quad \tau = \omega t, \quad \epsilon = \frac{\varepsilon k}{M\omega^2}, \quad h = \frac{\hbar k^2}{M\omega},$$
$$\mu = \frac{\Omega}{\omega} = N + \delta. \tag{3}$$

Here h is a dimensionless Planck constant, N is the (positive integer) resonance number, and δ is the detuning from the resonance.

The classical analog of the Hamiltonian (2) is

$$H = \frac{X^2}{2} + \frac{P^2}{2} + \epsilon\cos(X-\mu\tau), \tag{4}$$

where $P = kp/M\omega$ is the dimensionless momentum. In the action-angle variables (I,ϑ), the classical Hamiltonian (4) takes the form

$$H = I + \epsilon\cos[kr(I)\sin\vartheta - \mu\tau], \tag{5}$$

where $X = kr(I)\sin\vartheta$, $P = kr(I)\cos\vartheta$, $kr = \sqrt{X^2+P^2} = \sqrt{2I}$ is the dimensionless amplitude of oscillations, I is the dimensionless action measured in units of $I_0 = M\omega/k^2$, and ϑ is the phase of oscillations.

III. CONNECTION WITH A 2D SOLID-STATE LOCALIZATION PROBLEM

We write the solution to the Schrödinger equation

$$ih\frac{\partial\Psi(X,\tau)}{\partial\tau} = \hat{H}\Psi(X,\tau) \tag{6}$$

in the form of a series over the eigenfunctions $|n\rangle \equiv \phi_n(X)$ of the harmonic oscillator Hamiltonian $\hat{H}_0$,

$$\Psi(X,\tau) = \sum_{n=0}^{\infty} c_n(\tau)|n\rangle. \tag{7}$$

Then we obtain the equations for the complex amplitudes $c_n(\tau)$,

$$ih\frac{dc_m(\tau)}{d\tau} = h(m+1/2)c_m(\tau) + \epsilon\sum_{n=-m}^{\infty}\langle m|\cos(X-\mu\tau)|m+n\rangle c_{m+n}(\tau) \tag{8}$$
$$= h(m+1/2)c_m(\tau) + \frac{\epsilon}{2}\sum_{n=-m}^{\infty}(e^{-i\mu\tau}F_{m,m+n} + e^{i\mu\tau}F^*_{m,m+n})c_{m+n}(\tau).$$

In Eq. (8), $F_{m,m+n}$ is the matrix element [4],

$$F_{m,m+n} = \langle m|e^{iX}|m+n\rangle = \frac{i^n h^{n/2}e^{-h/4}}{2^{n/2}\sqrt{(m+1)(m+2)\cdots(m+n)}}L_m^n\left(\frac{h}{2}\right), \tag{9}$$

where L_m^n is the Laguerre polynomial. When $m \gg 1$, the Laguerre polynomials can be expressed in terms of the Bessel functions J_n [4] as

$$L_m^n\left(\frac{h}{2}\right) = \left(\frac{2m}{h}\right)^{n/2}J_n(\sqrt{2mh}), \tag{10}$$

where the argument of the Bessel function, $\sqrt{2mh} = kr_m$, is the quantized dimensionless amplitude of oscillations of the harmonic oscillator. Using Eqs. (9) and (10) the matrix elements can be written in the form

$$F_{m,m+n} = \frac{i^n m^{n/2}e^{-h/4}}{\sqrt{(m+1)\cdots(m+n)}}J_n(\sqrt{2mh}). \tag{11}$$

Since the Hamiltonian (2) is periodic in time the solution of the Schrödinger equation (8) can be written as

$$c_m^q(\tau) = e^{-i\sigma_q\tau/h}A_m^q(\tau), \tag{12}$$

where σ_q is a quasienergy, measured in units of $M\omega^2/k^2$, $c_m^q(\tau)$ is the quasienergy (QE) function, and $A_m^q(\tau)$ is a periodic function with the period $T = 2\pi/\mu$,

$$A_m^q(\tau + 2\pi/\mu) = A_m^q(\tau). \tag{13}$$

The quasienergy functions are the eigenfunctions of the evolution operator $\hat{U}$ for one period T of the external field,

$$\hat{U}(T)c_m^q(\tau) = e^{-i\sigma_q T/h}c_m^q(\tau). \tag{14}$$

The evolution operator for one period of the external field $\hat{U}(T)$ is

$$\hat{U}(T) = \hat{T}e^{-i\int_0^T\hat{H}(\tau)d\tau}, \tag{15}$$

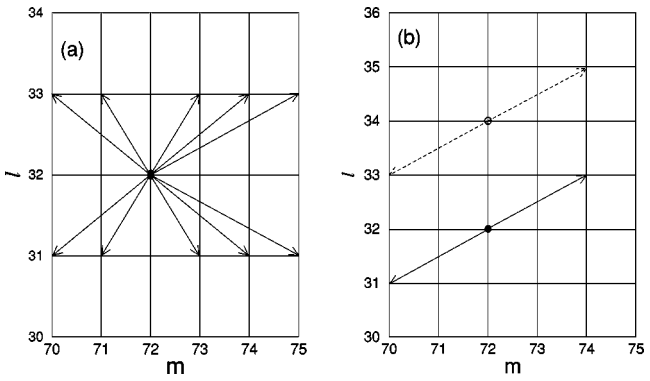

FIG. 1. (a) Some possible transitions on a 2D lattice given by Eq. (18). (b) Possible transitions on a 2D lattice at small ϵ, given by Eq. (24); $N=2$.

where $\hat{T}$ is the ordering operator, and $\hat{H}(\tau)$ in our problem is given by Eq. (2). In our numerical calculations, presented below, we consider only the QE states at the time $\tau=0$, so that $c_m^q(0)=A_m^q(0)\equiv A_m^q$.[1]

Substitution of Eq. (12) in Eq. (8) gives the equation for A_m^q:

$$\sigma_q A_m^q(\varphi)=-ih\mu\frac{dA_m^q(\varphi)}{d\varphi}+h(m+1/2)A_m^q(\varphi)+\frac{\epsilon}{2}\sum_{n=-m}^{\infty}(e^{-i\varphi}F_{m,m+n}+e^{i\varphi}F_{m,m+n}^{*})A_{m+n}^q(\varphi),\quad \varphi\equiv\mu\tau. \tag{16}$$

Expanding the function $A_m^q(\varphi)$ in a Fourier series,

$$A_m^q(\varphi)=\sum_{l=-\infty}^{\infty}A_{m,l}^q e^{-il\varphi}, \tag{17}$$

we derive the following equation for the amplitudes $A_{m,l}^q$:

$$E_q A_{m,l}^q=h(m-\mu l)A_{m,l}^q+\frac{\epsilon}{2}\sum_{n=-m}^{\infty}(F_{m,m+n}A_{m+n,l+1}^q+F_{m,m+n}^{*}A_{m+n,l-1}^q), \tag{18}$$

where $E_q=\sigma_q-h/2$.

Equation (18) can be interpreted as a problem of electron localization on a 2D lattice. Indeed, one can consider the complex coefficients $A_{m,l}^q$ as the complex amplitudes of the probability of finding an electron on a 2D lattice at the site (m,l), where $0\leqslant m<\infty$, $-\infty<l<\infty$. Some possible transitions in the system (18) are shown in Fig. 1(a). The particle, initially located at the site with indices (m_0,l_0), can jump to the sites $(m_0\pm n,l_0\pm 1)$, where n is an integer number.

[1]If the spectrum σ_q and QE functions A_m^q are known, one can trace the evolution of the quantum system at the times $\tau_s=sT$, where $s=0,1,2\ldots$ (see, for example [5]).

IV. THE RESONANCE APPROXIMATION

When the interaction amplitude is small, $\epsilon\ll 1$, the 2D solid state model described by Eq. (18) can be reduced to a 1D system, i.e., it can be described by an equation with only one index. We divide both parts of Eq. (18) by μ and, taking into account that $\delta\ll N$ and $1/\mu\approx 1/N-\delta/N^2$, we obtain

$$\frac{E_q}{\mu}A_{m,l}^q=h\left(\frac{m}{N}-\frac{\delta m}{N^2}-l\right)A_{m,l}^q+\frac{\epsilon}{2\mu}\sum_{n=-m}^{\infty}(F_{m,m+n}A_{m+n,l+1}^q+F_{m,m+n}^{*}A_{m+n,l-1}^q). \tag{19}$$

We assume that δ is small, so that $\delta m/N^2\ll 1$ for all considered values of m, or $\delta=0$. Then, in the zeroth order approximation we have from Eq. (19),

$$\left(\frac{m}{N}-l\right)A_{m,l}^q=\frac{E_q^{(0)}}{\mu h}A_{m,l}^q. \tag{20}$$

It follows from Eq. (20) that if $A_{m,l}^q\neq 0$ then $E_q^{(0)}/\mu h=(m/N)-l$. Since the ratio $E_q^{(0)}/\mu h$ is defined by modulus 1 [see Eq. (14)], we can write, $E_q^{(0)}/\mu h=0$.[2] Then Eq. (20) takes the form

$$(m-Nl)A_{m,l}^q=0. \tag{21}$$

Hence,

$$A_{m,l}^q=0 \quad \text{for} \quad m\neq Nl, \tag{22}$$

$$A_{m,l}^q\equiv A_m^q \quad \text{for} \quad m=Nl. \tag{23}$$

The next order approximation for $m=Nl$ yields

$$(E_q-h\,\delta m/N)A_m^q=\frac{\epsilon}{2}(F_{m,m+N}A_{m+N}^q+F_{m,m-N}^{*}A_{m-N}^q), \tag{24}$$

where $E_q=E_q^{(1)}$ (we do not consider the higher order approximations). As one can see from Eq. (21), in the m direction only hops of distance N are allowed. Thus, the 2D problem, given by Eq. (18), is reduced in the case $\epsilon\ll 1$ to the 1D problem described by Eq. (24).

The localization properties of the quantum states in the resonance approximation, given by Eq. (24), are defined by the structure of the matrix elements $F_{m,m+N}$. If the matrix elements are periodic functions of m, all the eigenstates are extended and the spectrum is continuous. This situation is common for solid-state systems [6]. In the system under consideration, the matrix elements (11) are nonperiodic. For this

[2]We assume that $(m/N)-l$ is an integer for some initial state m_0. If not, one may introduce the quasienergy $E_q'=E_q-\mu h\{m_0/N\}$ and a new index $m'=m-\{m_0/N\}N$, and solve Eqs. (19) and (20) for E_q' and m' instead of E_q and m. Here $\{x\}$ is the fractional part of x.

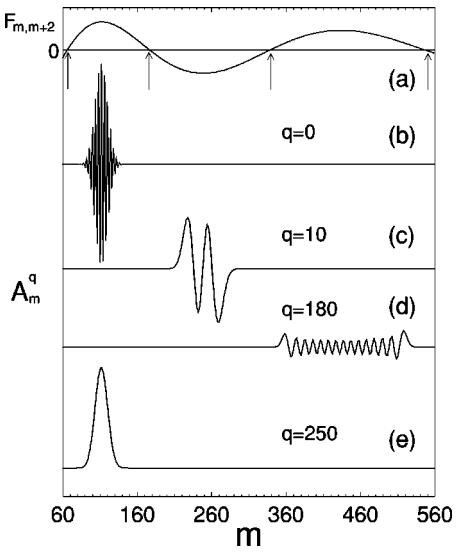

FIG. 2. (a) The matrix elements (in arbitrary units), and (b)–(e) some characteristic QE functions, given by Eq. (24) with $h=0.2$, $\epsilon=0.02$, $\delta=0$, $N=2$. Only even values of m are included.

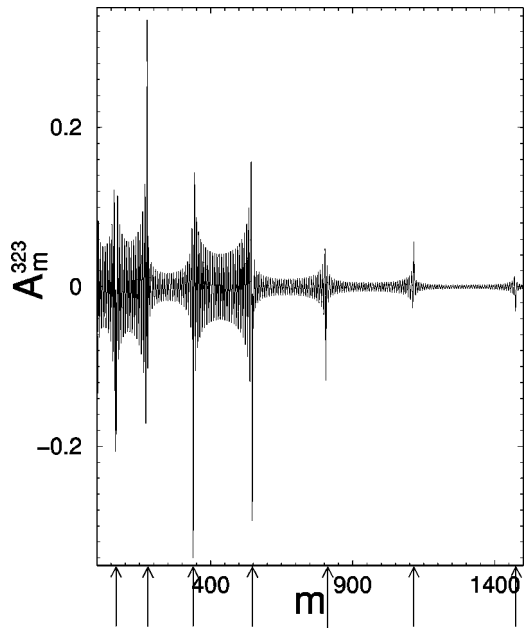

FIG. 3. The characteristic QE functions delocalized over several resonance cells (at even m); $q=323$, $N=2$, $h=0.2$, $\epsilon=0.02$, $\delta=0$.

reason, as will be shown below (see also Refs. [5,7]), the quantum states are localized and the spectrum is discrete.

The matrix elements given by Eq. (11) oscillate as a function of m. At the points m_0 where the matrix elements are close to zero,

$$F_{m_0,m_0+N}\sim J_N(\sqrt{2m_0h})\approx 0, \tag{25}$$

the transition probability is very small. As a consequence, such points becomes the dynamical barriers to the probability flow [7], and divide the Hilbert space, labeled by the index m, into relatively independent parts—resonance cells [8]. Most of the eigenstates given by Eq. (24) are concentrated inside these cells. The localization length λ_i for the states in the ith cell does not exceed the size of the cell. The cell boundaries are defined by Eq. (25), i.e., $\lambda_i \leqslant m_{i+1}-m_i$, where m_i and m_{i+1} satisfy Eq. (25), so that $\sqrt{2m_ih}$ and $\sqrt{2m_{i+1}h}$ are, respectively, the ith and $(i+1)$th roots of the Bessel function in Eq. (25).

Some characteristic QE functions given by Eq. (24) are illustrated in Figs. 2(b)–2(e) for small ϵ. The boundaries of the resonance cells are marked by arrows. One can see from Figs. 2(b)–2(e) that the eigenfunctions are localized inside the cells, but, on the other hand, each eigenfunction is delocalized over m inside a single cell. For example, for the initial states in Fig. 1(b) with $m=72$ the transitions will occur in the region $66<m<176$ [inside the first cell in Fig. 2(a)]. Note that for small values of ϵ and when $\delta=0$ the localization properties of our system are independent of ϵ. This means that an arbitrarily small perturbation ϵ initiates transitions between the sites on the effective rectangular lattice. For small values of ϵ, these transitions take place on the 1D sublattices shown in Fig. 1(b).

Except for the localized (in the resonance cells) eigenfunctions there exist a few eigenfunctions that are delocalized over several resonant cells. One of these representative eigenfunctions is shown in Fig. 3. The QE functions delocalized over several resonant cells have maxima in the regions near the boundaries of the cells marked in Fig. 3 by arrows. Thus, if the initial state is located near the boundary of a resonance cell, say, at $m=66$ in Figs. 2 and 3 (in the region near the first arrow), then this state will propagate for a large distance in m, over the 1D sublattice. This distance can be much larger than the size of the single resonance cell [5].

The structure of the QE states can be better understood from the plot of the means of the QE functions, $m_q=\Sigma_m|A^q_m|^2m$, versus their variances $\Delta_q=[\Sigma_m|A^q_m|^2(m-m_q)^2]^{1/2}$, presented in Fig. 4(a). Each eigenfunction A^q_m is represented by one point in the figure. One can see that most of the eigenfunctions are localized inside the resonance cells since their means are located inside the cells and their variances do not exceed the size of the cell. Each row in the figure is formed by the eigenfunctions of one cell. If the

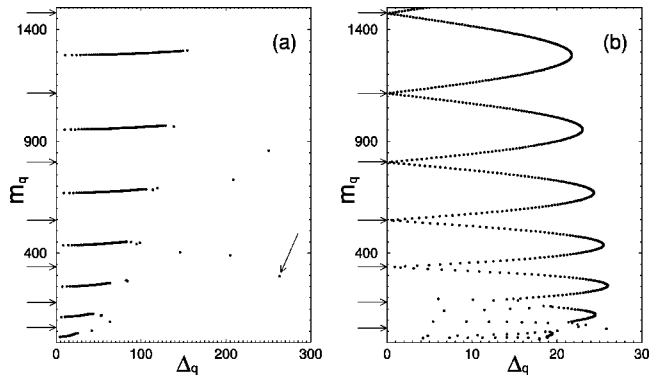

FIG. 4. The plot of m_q versus Δ_q for $N=2$, $h=0.2$, $\epsilon=0.02$, and (a) $\delta=0$, (b) $\delta=0.001$. The boundaries of the resonance cells are marked by the arrows on the m_q axis.

initial state is located inside the resonance cell, the eigenfunctions of this particular cell define the quantum dynamics. These states make the quantum dynamics localized inside the cell and, at the same time, delocalized over the states m inside the cell [7]. In the corresponding solid-state model (24), the localization length for the states, in ith cell at small ϵ can be identified with the size of this resonance cell; namely, $\lambda_i = m_{i+1} - m_i$, where $\sqrt{2m_i h}$ and $\sqrt{2m_{i+1}h}$ are two successive roots of the Bessel function (25).

The QE functions delocalized over several resonant cells are represented in Fig. 4(a) by the scattered points with large variances. One such function, marked in Fig. 4(a) by an arrow, is shown in Fig. 3. The QE functions delocalized over several resonant cells cannot be attributed to a definite resonance cell since their variances are larger than the size of single cells. As a consequence, these functions cause delocalization of the states initially concentrated near the boundaries of the cells. However, as shown in Ref. [7], the localization length remains finite, because the matrix elements (11) are nonperiodic and their amplitudes decrease with increasing m (as $m^{-1/4}$ at $m \gg 1$).

In the case when the detuning from the resonance [see Eq. (3)] is not equal to zero ($\delta \neq 0$), the character of the localization depends on the position of the initial state m_0 [see Fig. 4(b)]. In the region $m_0 \geqslant m_{max} = \epsilon N/h\delta$ all the states remain exponentially localized in m, since in this case Eq. (24) has the solution

$$E_q = (h\delta m/N)\,\delta_{m,q}, \quad A_m^q = \delta_{m,q}. \tag{26}$$

If $m_0 \ll m_{max}$ the above discussed effect of localization over the resonance cells takes place. In the intermediate case, when $m_0 \geqslant m_{max}$, the character of the localization depends on the position of the state m_0 inside the resonance cell. [For the parameters in Fig. 4(b) $m_{max} = 200$.] If m_0 is located near the boundary of the resonance cell where the condition (25) is satisfied, Eq. (24) has the localized solution (26). Most delocalized functions have their mean m_q at the center of a resonance cell.

As follows from Fig. 4(b), in the region $m_0 \geqslant m_{max}$ the QE functions delocalized over several resonant cells are absent, since the variance of each function is much less than the size of the cell, whose boundaries are marked in Fig. 4(b) by arrows. Moreover, the variances of the eigenstates in the near-resonance case in Fig. 4(b) are substantially smaller than the variances in the exact resonance case shown in Fig. 4(a). Hence, at small ϵ, an increase of the value of the detuning δ always leads to localization of the quantum states in the model discussed.

Most of the localization properties of the eigenfunctions, given by Eq. (24), are the quantum manifestation of the classical behavior in phase space. The classical phase space in the variables $(kr(I), \theta)$, where $\theta = N\vartheta$, mod 2π, generated by the exact classical Hamiltonian (5), is shown in Fig. 5(a) for the exact resonance case ($\delta = 0$) and in Fig. 5(b) for the near-resonance case ($\delta = 0.001$).

As one can see from Fig. 5(a), in the case $\delta = 0$ the classical phase space is divided into resonance cells. [Figure 5(a) shows only the first seven cells.] The boundaries of the cells,

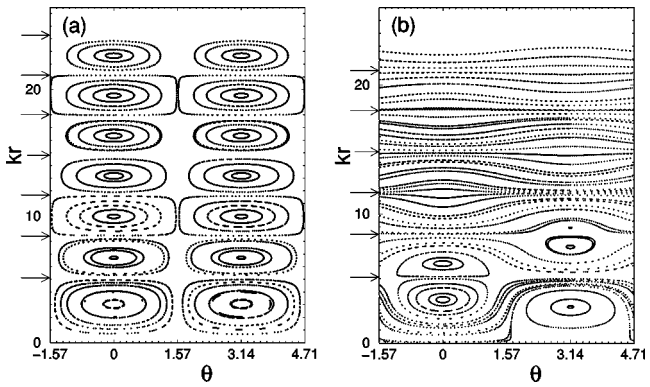

FIG. 5. The classical phase space for (a) $\delta = 0$, (b) $\delta = 0.001$; $N = 2$, $\epsilon = 0.02$. The boundaries of the resonance cells are marked by arrows.

$kr(I_i) = \sqrt{2I_i}$, are marked in Figs. 5(a) and 5(b) by arrows. As shown in Refs. [8,9], in the quasiclassical limit the ith boundary of the classical cell kr_i in Figs. 5(a) and 5(b) corresponds to the ith boundary of the quantum cell m_i on the m_q axis in Figs. 4(a) and 4(b), so that $kr_i = \sqrt{2I_i} = \sqrt{2hm_i}$.

Each row of points in Fig. 4(a) is formed by the eigenstates responsible for the dynamics in the corresponding quantum cell. From comparison with the classical dynamics in phase space we can now describe the localization properties of the quantum states discussed above. Each value of m in the quantum system corresponds to a quantized classical action $I_m = mh$, or to the quantized dimensionless oscillation amplitude $kr_m = \sqrt{2mh}$. Each value of action I_m (or kr_m) corresponds to a set of classical trajectories. Moving along some classical trajectory the particle with some initial value of action I_m can accept other values in the interval $I_{m_1} < I_m < I_{m_2}$. The corresponding eigenstate will be delocalized over the unperturbed states with numbers m in the interval $m_1 < m < m_2$. From the form of the trajectories in Fig. 5(a) one can see that in the case of exact resonance all quantum states of the single quantum cell should be delocalized over the resonance cell, since in the phase space both the extremal values I_{m_1} and I_{m_2} that limit the resonance cell can belong to the same trajectory.

Similar arguments can be used to analyze the quantum-classical correspondence in the near-resonance case. As follows from Fig. 5(b), at $\delta \neq 0$ in the phase space there is only a finite number of resonance cells [two cells in Fig. 5(b)]. Thus, there is a finite number of quantum resonance cells in the Hilbert space in Fig. 4(b) (the first two cells). In the off-resonant region [third to seventh cells in Fig. 4(b)] the degree of delocalization of eigenstates depends on the position of the state in the cell destroyed by the finite detuning δ. In Fig. 5(b) the least curved trajectories are located near the separatrices, while the the most curved trajectories are located near the centers of the destroyed cells. As a consequence, in the quantum model the eigenfunctions in Fig. 5(b) have their smallest variance in the region near the separatrices and their largest variance near the centers of the destroyed cells.

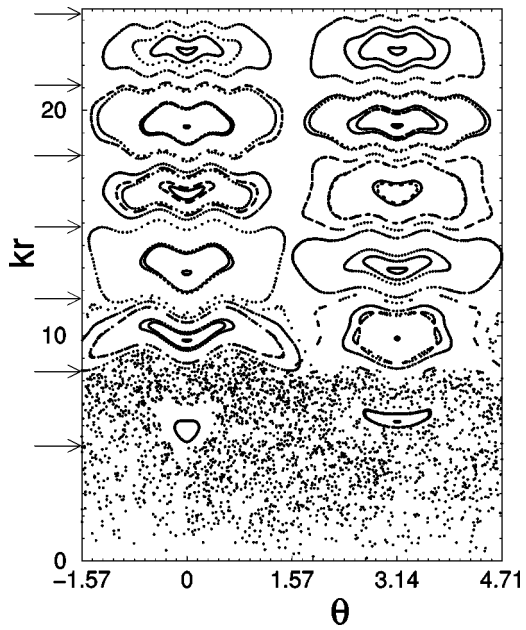

FIG. 6. The classical phase space in the case $\epsilon=3$. Other parameters are $\delta=0$, $N=2$. The boundaries of the resonance cells are marked by arrows.

V. THE LOCALIZATION LENGTH IN THE CASE OF STRONG INTERACTION

In the previous sections we considered the dynamics only at small perturbation amplitude $\epsilon \ll 1$. At large values of ϵ dynamical chaos appears in the classical [10] and quantum [5,11] monochromatically perturbed oscillators. As will be shown below, all quantum states in the chaotic area are delocalized over the whole chaotic region. The chaotic dynamics in the monochromatically perturbed oscillator corresponds to hops in different directions in the solid-state system, as shown in Fig. 1(a). By estimating the size of the chaotic motion in the monochromatically perturbed oscillator we will estimate below the localization length in the corresponding solid-state model.

In Fig. 6 the classical phase space is shown for $\epsilon=3$. One can see that in the first two cells the motion is mainly chaotic while in the other cells the motion remains mainly regular. The time-averaged quantum probability distribution $\overline{|C_m(\tau)|^2}$ is illustrated in Fig. 7(a) for the case of small ϵ and in Fig. 7(b) for the case $\epsilon=3$. The initial state was taken in the form $c_m(0)=\delta_{m,m_0}$ with $m_0=30$ [in the center of the first cell in Figs. 7(a) and 7(b)]. As follows from Fig. 7(a), the quantum particle can tunnel (see also Ref. [7]) from the initial (first) cell to other resonance cells, unlike the classical case, where essentially all the trajectories in the phase space are confined inside the resonant cells [see Fig. 5(a)].

When ϵ increases, the probability distribution in Fig. 7(b) increases in most of the quantum cells, which corresponds to chaotization of motion in the classical phase space. In Fig. 8(a) we show the plot $m_q(\sigma_q)$ for the case $\epsilon=3$, and in Fig. 8(b) the characteristic QE function located in the chaotic area is illustrated. As one can see from Fig. 8(a), almost all QE states in the area of the first two cells are delocalized over both the cells. In other words, the QE states are localized

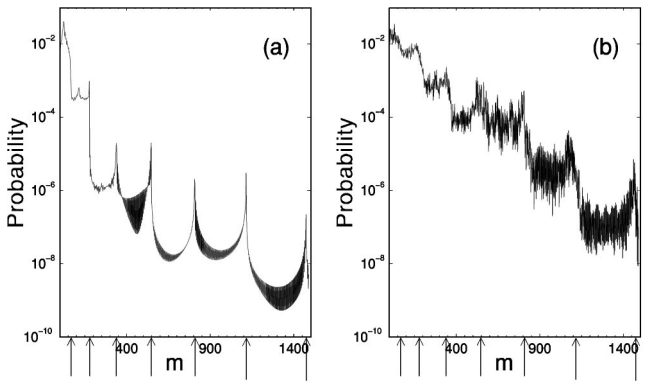

FIG. 7. The time-averaged probability distribution. (a) $\epsilon=0.02$; the averaging has been performed over 100 realizations in the time interval $\tau=5000-105\,000$ (only the probability at even m is shown). (b) $\epsilon=3$, where the averaging has been performed over 100 realizations in the time interval $\tau=500-10500$. Other parameters are $h=0.2$, $\delta=0$, $N=2$. The boundaries of the resonance cells are marked by arrows.

inside the chaotic area (first two cells), but not inside the single cells, as in the case of small ϵ in Fig. 4(a). In the chaotic regime, one can find a quantum particle with equal probability in any unperturbed state m inside the chaotic sea, independently of the position and form of the initial state located in this region [see the first two cells in Figs. 7(b), 8(a), and 8(b)]. When ϵ increases, more classical and quantum cells become chaotic. This results in increasing the area of delocalization of the quantum chaotic states. Thus, in the regime of chaos the localization length in the solid-state system may be identified with the size of the chaotic area in the monochromatically perturbed oscillator. For example, for the parameters in Figs. 6, 8(a), and 8(b) the localization length for the states in the chaotic region is $\lambda=m_2$, where $\sqrt{2m_2h}$ is the second root of the Bessel function in Eq. (25). [The value m_2 is marked by the second arrow in each of Figs. 6, 8(a), and 8(b).]

It is necessary to note that, as was shown in [11], the quantum and classical dynamics in the chaotic regime are essentially independent of the detuning δ when $\epsilon \gg \delta$. So the

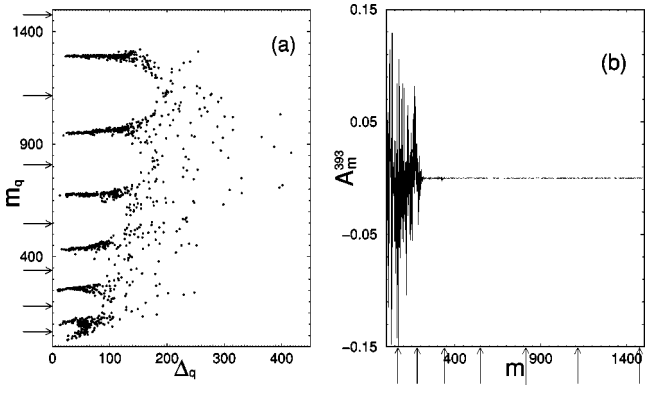

FIG. 8. (a) The plot of m_q versus σ_q and (b) the characteristic QE eigenfunction located in the chaotic region for $\epsilon=3$ and $h=0.2$, $\delta=0$, $N=2$. The boundaries of the resonance cells are marked by arrows.

results concerning the chaotic dynamics valid in the near-resonance case also remain when $\delta \neq 0$.

VI. EXPERIMENTAL APPLICATIONS

The localization properties of the monochromatically perturbed oscillator, discussed in this paper, allow us to describe the stability of an ion trapped in a linear ion trap. The ion can be cooled down to the ground state of the trapping potential by the standard Doppler cooling and by the optical pumping method. The external laser fields, which influence the electron transitions, result in perturbation of the vibrational dynamics of the ion. This leads to heating of the ion in the trap. As shown below, the effective temperature of the ion is defined by the value of the localization length.

Let us represent the probability distribution of the ion in the form $P_n(\mathcal{T}) = |C_n|^2 = \exp(-\hbar\omega n/\mathcal{T})$, where $\mathcal{T}$ is the temperature measured in energy units and the index n labels the energy level of the unperturbed ion. In dimensionless units the probability can be rewritten as $P_n(\Theta) = \exp(-hn/\Theta)$, where the dimensionless temperature $\Theta = \mathcal{T}/(M\omega^2/k^2)$ is measured in the same units as the dimensionless wave amplitude ϵ. On the other hand, one can express the probability distribution P_n through the localization length λ as $P_n(\lambda) = \exp(-n/\lambda)$. For example, for ionized calcium with $M = 6.64 \times 10^{-23}$ g, $\omega = 2\pi \times 500$ kHz, and $k = 1.58 \times 10^5$ cm^{-1}, the localization length $\lambda = 20$ corresponds to the dimensionless temperature $\Theta = h\lambda = 2.4$, or to the temperature 4.6×10^{-4} K. Increasing the wave amplitude ϵ results in growth of the size of the chaotic region and in increasing the localization length λ. As a consequence, the temperature of the system increases.

VII. CONCLUSION

The regular and chaotic classical and quantum dynamical regimes are analyzed in the system of an ion trapped in a linear ion trap and interacting with two laser fields with close frequencies. This system is modeled using a quantum oscillator perturbed by a monochromatic wave. Since the spectrum of the harmonic oscillator is linear, the two-dimensional lattice in the Hilbert space for the monochromatically perturbed oscillator is uniform, which allows formulatation of the problem of dynamical stability in this system in terms of the problem of electron localization in a 2D solid-state system. The resonance approximation is used to decrease the effective dimensionality of the corresponding solid-state system. This can be done in the case of a relatively small interaction between the trapped ion and the laser fields. In the solid-state model this case corresponds to weak interaction between the sites of the 2D lattice. Increasing the interaction amplitude results in delocalization of the quantum states over the sites of the 2D cell. The area of delocalization in the solid-state system for strong interaction in the chaotic area may be identified with the size of the chaotic sea in the monochromatically perturbed oscillator. Our results provide understanding of the mechanism of stability of an ion trapped in a linear ion trap. They also allow one to estimate the characteristic dynamical regimes of the trapped ion and to choose parameters required for dynamical stability. We show that the value of the localization length λ characterizes an experimentally measurable parameter—the temperature of the ion.

ACKNOWLEDGMENTS

We thank G. Chapline for useful discussions. This work was supported by the Department of Energy (DOE) under Contract No. W-7405-ENG-36, by the National Security Agency (NSA), and by the Advanced Research and Development Activity program (ARDA).

[1] F. Haake, *Quantum Signature of Chaos* (Springer-Verlag, New York, 1991).
[2] L.E. Reichl, *The Transition to Chaos* (Springer-Verlag, New York, 1992).
[3] G.P. Berman, D.F.V. James, R.J. Hughes, M. S. Gulley, M.H. Holzscheiter, and G.V. López, Phys. Rev. A **61**, 023403 (2000).
[4] I.S. Gradshteyn and I.M. Ryzhik, *Table of Integrals, Series, and Products* (Academic Press, New York, 1980).
[5] V.Ya. Demikhovskii, D.I. Kamenev, and G.A. Luna-Acosta, Phys. Rev. E **59**, 294 (1999).
[6] M. Kohmoto and Y. Hatsugai, Phys. Rev. B **41**, 9527 (1990).
[7] V.Ya. Demikhovskii and D.I. Kamenev, Phys. Lett. A **228**, 391 (1997).
[8] V.Ya. Demikhovskii, D.I. Kamenev, and G.A. Luna-Acosta, Phys. Rev. E **52**, 3351 (1995).
[9] G.P. Berman, V.Ya. Demikhovskii, and D.I. Kamenev, Chaos **10**, 670 (2000).
[10] G.M. Zaslavskii, R.Z. Sagdeev, D.A. Usikov, and A.A. Chernikov, *Weak Chaos and Quasiregular Patterns* (Cambridge University Press, Cambridge, 1991).
[11] G.P. Berman, D.F.V. James, and D.I. Kamenev, Chaos **10**, 371 (2000).